THE ASTROPHYSICAL JOURNAL, 555:563–571, 2001 July 10

THE COSMIC INFRARED BACKGROUND AT 1.25 AND 2.2 MICRONS USING DIRBE AND 2MASS: A CONTRIBUTION NOT DUE TO GALAXIES?

L. CAMBRÉSY AND W. T. REACH
Infrared Processing and Analysis Center, California Institute of Technology, M/S 100-22, Pasadena, CA 91125;
laurent@ipac.caltech.edu, reach@ipac.caltech.edu

C. A. BEICHMAN
Jet Propulsion Laboratory, California Institute of Technology, M/S 180-703, Pasadena, CA 91109; chas@pop.jpl.nasa.gov

AND

T. H. JARRETT
Infrared Processing and Analysis Center, California Institute of Technology, M/S 100-22, Pasadena, CA 91125; jarrett@ipac.caltech.edu
Received 2000 September 20; accepted 2001 March 6

ABSTRACT

Using the 2MASS second incremental data release and the zodiacal subtracted mission average maps of *COBE*/DIRBE, we estimate the cosmic background in the J (1.25 μm) and K (2.2 μm) bands using selected areas representing ~ 550 deg^2 of sky. We find a J background of 22.9 ± 7.0 kJy sr^{-1} (54.0 ± 16.8 nW m^{-2} sr^{-1}) and a K background of 20.4 ± 4.9 kJy sr^{-1} (27.8 ± 6.7 nW m^{-2} sr^{-1}). This large-scale study shows that the main uncertainty comes from the residual zodiacal emission. The cosmic background we obtain is significantly higher than integrated galaxy counts (3.6 ± 0.8 kJy sr^{-1} and 5.3 ± 1.2 kJy sr^{-1} for J and K, respectively), suggesting either an increase of the galaxy luminosity function for magnitudes fainter than 30 mag or the existence of another contribution to the cosmic background from primeval stars, black holes, or relic particle decay.

Subject headings: cosmology: observations — diffuse radiation — infrared: general

1. INTRODUCTION

The cosmic infrared background (CIB) is an important cosmological constraint on star formation history in the universe (Dwek et al. 1998; Gispert, Lagache, & Puget 2000). The first detection of the CIB was reported by Puget et al. (1996) for submillimetric wavelengths using data from the Far Infrared Absolute Spectrometer on board the *Cosmic Background Explorer* (*COBE*). Shorter wavelengths have been investigated with the help of the *COBE* Diffuse Infrared Background Experiment (DIRBE) from 240 μm to 1.25 μm. Hauser et al. (1998a) measured the CIB at 240 and 140 μm and set upper limits for other wavelengths. Lagache et al. (2000) proposed an estimation of the CIB at 100 μm.

The CIB is the signal that remains after subtracting the emission from the interstellar medium, stars, and interplanetary dust (scattering and emission) from the total celestial brightness. However, estimating the contamination due to these three foreground components is challenging. The interstellar medium is the main contaminant for long wavelengths, whereas starlight and zodiacal light dominate at the wavelengths studied in the present paper ($J = 1.25$ μm and $K = 2.2$ μm).

Stellar population models were used to estimate the brightness of starlight in the large-beam DIRBE data (Arendt et al. 1998), but this technique led only to upper limits. The first detection of the CIB in the near-infrared (at 3.5 μm, L band) was proposed by Dwek & Arendt (1998) using DIRBE. Detections at 3.5 μm and 2.2 μm (K band) were reported by Gorjian, Wright, & Chary (2000) using near-infrared observations of a $2^\circ \times 2^\circ$ dark spot to measure the brightness of stars in a few DIRBE beams. Wright (2001) confirmed the result at 2.2 μm and proposed a weak limit for 1.25 μm (J band) using data from the 2 Micron All-Sky Survey (2MASS) for four dark spots. Matsumoto et al. (2000) estimated the CIB from 1.4 μm to 4 μm with the Near Infrared Spectrometer (NIRS) on board the *Infrared Telescope in Space*. Although NIRS provided a point-source catalog limited to stars brighter than 7.5 mag at 2.24 μm, significant stellar contamination remains, and the CIB estimate is strongly dependent on the stellar population model used to remove the contribution from fainter stars.

This work presents a large-scale study of the CIB using 2MASS data for 1400 deg^2 of the sky in order to accurately estimate the stellar contribution to the surface brightness observed by DIRBE. The 2MASS and DIRBE data are described in § 2; the method used to compare these two data sets is presented is § 3; § 4 presents the determination of the CIB for J and K with the associated uncertainties; and § 5 is dedicated to comparisons with previous results and with galaxy counts.

2. DATA

2.1. *2MASS*

The second incremental data release from the 2MASS survey covers 48% of the sky and contains 1.6×10^8 stars (Cutri et al. 2000). The Point Source Catalog completeness limits are 15.8 and 14.3 mag with a signal-to-noise ratio greater than 10:1 for J and K_s, respectively. No photometry is provided for stars brighter than 4–5 mag (see § 3.2).

Since the catalog of the whole release is ~ 7 Gbytes in binary format, we choose to work on integrated maps in which each pixel corresponds to the integrated flux in a $5' \times 5'$ box. These maps are constructed from the point-source catalog clipped to remove sources fainter than the completeness limit. Magnitudes are converted to flux density using the flux for zero magnitude $F_0(J) = 1603$ Jy, as defined by Campins, Rieke, & Lebofsky (1985), and $F_0(K_s) = 698$ Jy, which is an extrapolation of the J value to the K_s filter, assuming a blackbody at 9700 K (Vega photo-

metric system). Uncertainties on these photometric zero points are about 2% and do not affect our results. Each $5' \times 5'$ box contains the sum of the point-source fluxes in the area.

The resulting image in an Aitoff (equal area) projection consists of 4321×2161 pixels. This size is reasonable, and the image can be handled globally. Errors resulting from this pixelization are negligible since $5'$ is small compared to the DIRBE beam of 1° (see below).

We should point out that the 2MASS K_s filter (2.17 μm) and the DIRBE K filter (2.2 μm) are slightly different. Persson et al. (1998) discuss the K to K_s transformation and present a list of photometric standards in both colors. Moreover, as Pahre & Mould (1994) point out, the K_s bandpass is intermediate between K and K', and rough corrections of K_s to K can be obtained by averaging K' and K. This transformation is well defined by Wainscoat & Cowie (1992): $K'-K = (0.22 \pm 0.03)(H-K)$ for $0 < H-K < 0.4$ ($K'-K \sim 0.07$ otherwise). For example, for a K5 spectral type star, we would obtain $K_s-K \sim 0.01$. This correction is negligible compared to uncertainties described further in the paper, and differences between 2MASS and DIRBE filters will be ignored in the following analysis.

2.2. *DIRBE*

Cryogenic DIRBE operation took place from 1989 December to 1990 September. During these 10 months, the sky was observed at the rate of half of the sky per week in 10 bands, from 1.25 μm to 240 μm (Hauser et al. 1998a). The DIRBE instrument was designed to make accurate absolute sky-brightness measurements, with a stray light rejection of less than 1 nW m^{-2} sr^{-1} and an absolute brightness calibration uncertainty of 0.05 and 0.03 nW m^{-2} sr^{-1}, at 1.25 and 2.2 μm, respectively.

The zodiacal light is the first component along the line of sight and must be removed using an interplanetary dust model (e.g., Kelsall et al. 1998). However, these models are not unique (see Wright 1998 and Gorjian et al. 2000 for another model). Artifacts still remain. In the following analysis, we use the zodiacal subtracted mission average (ZSMA) maps produced by the DIRBE team (Hauser, Kelsall, & Weiland 1998b). The zodiacal light intensities were subtracted week by week, and the residual intensity values were averaged to create the ZSMA maps.

To compare DIRBE and 2MASS, we need precise knowledge of the DIRBE beam in both J and K bands. The $42'$ beam size commonly mentioned in the literature is only valid for daily maps, not for the annual maps used here. The beam for the J band is presented in Figure 1. This is an effective beam profile (provided with DIRBE maps), which measures the relative response of DIRBE to a point source, including the effects of sky scanning and data sampling rates. The beam for the annual maps corresponds to an average of the effective beam for all orientations (Fig. 1). Similar results are obtained for J and K, and the full width at half-maximum (FWHM) of both beams is $\sim 1^\circ$ (solid angle ~ 0.78 deg^2).

3. METHOD

3.1. *2MASS Integration on DIRBE Pixels*

First, we exclude from this study regions of the sky for which we know that the CIB cannot be straightforwardly extracted because of, e.g., high stellar density, interstellar cirrus (which is responsible for emission and scattering), and residual zodiacal light structures in the DIRBE maps.

We keep only regions that satisfy the following criteria: (1) high Galactic latitude: $|b| > 40^\circ$, (2) low DIRBE 240 μm flux in order to eliminate diffuse emission or scattered light from cirrus clouds: $I_{240} < 3$ MJy sr^{-1}, (3) high ecliptic latitude: $|\beta| > 30^\circ$, and (4) exclusion of the Magellanic Clouds.

The most straightforward way to remove the stellar component (2MASS) from the DIRBE flux is to work directly in the *COBE* coordinate system (projection on a cube) and to integrate the 2MASS maps on each DIRBE pixel. However, since the 2MASS data still contain coverage holes, we keep only those that are completely covered by 2MASS. The effective useful region covers, finally, about 1400 deg^2 (Fig. 2).

3.2. *Bright Stars*

In the remaining 1400 deg^2 piece of sky, $\sim 25\%$ of the pixels are contaminated by bright stars. Stars bright enough to be detected as point sources in DIRBE are saturated in 2MASS. Consequently their photometry cannot be derived from 2MASS to be subtracted from DIRBE.

Moreover, the DIRBE beam has a size of 1°, but the sampling of the data is $22'$. Therefore, several pixels are contaminated by a bright star, and this contamination depends on the star position in the beam. To identify pixels affected by these stars, we use a median filter that deals with the 2MASS holes. A pixel is considered contaminated if it is brighter than the threshold, $\mathcal{T}$, defined by the median plus $2\,\sigma$, $M + 2\,\sigma$, of the surrounding pixels in a 3° radius circle

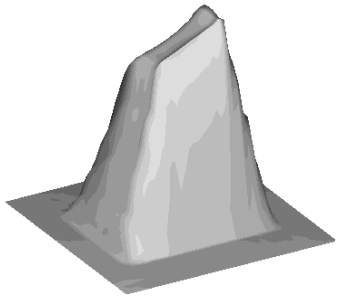

FIG. 1*a*

FIG. 1*b*

FIG. 1.—(*a*) Effective DIRBE beam for daily maps (FWHM = $42'$) at 1.25 μm. (*b*) Averaged beam for annual map (FWHM = 1°).

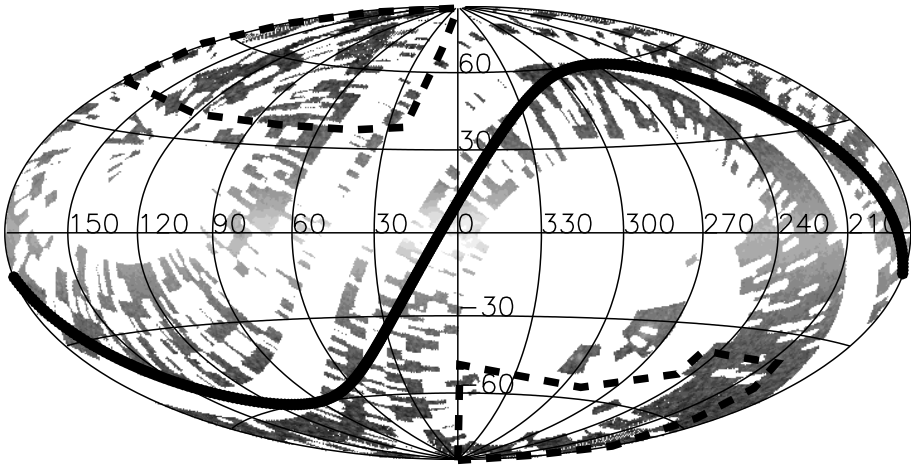

FIG. 2.—Aitoff projection in Galactic coordinates of the integrated 2MASS map (J) on DIRBE pixels. The large line represents the ecliptic plane. This study is limited to the areas inside the dashed curves (i.e., high Galactic and ecliptic latitudes); nonzero pixels correspond to ~ 1400 deg^2.

of the DIRBE − 2MASS map:

$$\mathcal{T}^i = M^i\left(\sum_{i,r=3^\circ} \text{DIRBE} - \text{2MASS}\right) + 2\,\sigma^i\left(\sum_{i,r=3^\circ} \text{DIRBE} - \text{2MASS}\right). \quad (1)$$

Pixels fainter than $M - (2\ \sigma)$ are also removed to avoid bias. In order to validate this operation, we use the 2MASS bright infrared star compilation (Tam et al. 1999[1]), which contains photometry for stars as bright as -4 mag in J, H, and K_s. This compilation consists of data taken from the literature and photometry extrapolations from *IRAS*, MSX, and 2MASS. Among the 343 stars brighter than $J = 5$ mag in our regions of interest, 11 are not identified with the median filter (eq. [1]). However, these remaining contaminated pixels are rejected by the robust linear fitting of DIRBE/2MASS brightness (see Fig. 4). After removing bright stars, 1040 deg^2 of the sky remains.

[1] See http://spider.ipac.caltech.edu/staff/raymond/2mass/birsc/birsc.html.

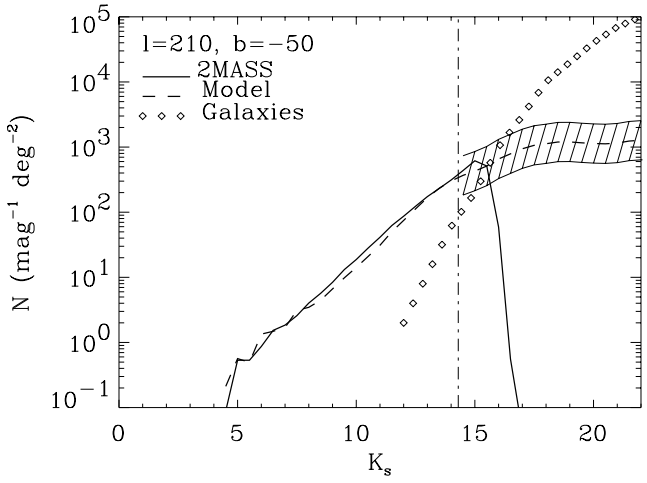

FIG. 3.—The K_s source counts from 2MASS (*solid line*) and from the model used for faint stars (*dashed line*) and galaxy counts (*diamonds*) from Gardner et al. (1997). Shaded area corresponds to the model uncertainties. The vertical line shows the cutoff used in the 2MASS catalog; the model provides us with counts for fainter magnitudes. Note that at this location ($l = 210^\circ$, $b = -50^\circ$) galaxies dominate the counts for $K_s > 16$.

3.3. *Faint Stars*

The 2MASS integrated brightness maps were limited to the formal completeness limits of 2MASS ($J^{\rm lim} = 15.8$ mag, $K_s^{\rm lim} = 14.3$ mag). A model is required to estimate the contribution of the fainter stellar population with respect to the position in the sky. We use a model in which the number and distribution of Milky Way stars, as seen in the near- to mid-infrared, is adapted from the Bahcall & Soneira (1980) optical star-count model. We have employed the discrete population formalism of Elias (1978), Jones et al. (1981), Garwood & Jones (1987), and Jarrett (1992). The model includes the class III (evolved giant), class IV (subdwarf), and class V (main sequence) stellar populations. These are further divided into disk and spheroid spatial distributions (see Bahcall & Soneira 1980). The stars are discretely binned according to their spectral types, ranging from the hottest O stars to the coolest M dwarfs, giving a total of 22 separate spectral bins for the main-sequence stars and 12 for the luminous giants (ranging from G2 to M7 giant). The optical/infrared colors, fluxes, and luminosity functions per spectral type are based on empirical data (e.g., Koornneef 1983; 2MASS, *ISO*, and *IRAS*). Interstellar extinction is applied as a smooth exponential function of Galactic position, characterized by scale height and disk length. The model parameters were tuned using deep optical and infrared star counts. The resultant model was validated using the 2MASS survey down to $J = 15$ and $K_s = 14$ mag (~ 2 mJy).

The result of the model for a typical high Galactic latitude field ($l = 210^\circ$, $b = -50^\circ$) is presented in Figure 3. As expected, 2MASS counts are complete to at least $K_s = 14.3$ mag. According to the model, less than 3% of the total stellar energy is contained in stars fainter than $K_s = 14.3$, and less than 0.1% of the total stellar energy is contained in stars fainter than $K_s = 19$. The model is useful for magnitudes ranging from 14.3 to ~ 20 in K_s. Assuming a conservative number-density uncertainty of a factor of 2 for these faint magnitudes, the resulting error will not exceed 3% of the total stellar flux.

4. RESULTS

4.1. *DIRBE/2MASS Correlation*

We choose four areas with a radius of 5° in order to illustrate the correlation between DIRBE and 2MASS. Pixels contaminated by bright stars have been filtered. Figure 4 shows the correlations for J and K bands. The main characteristics for each region are summarized in Table 1. We note that slopes are not exactly 1 ($\sim$1.07 for J, $\sim$0.94 for K). This arises from the different calibration strategy used by DIRBE and 2MASS: DIRBE is calibrated with Sirius while 2MASS is calibrated with a list of calibration stars of many different spectral types (Cutri et al. 2000). These calibration differences affect only the slope of the DIRBE/2MASS relation, not the value of the intercept, which is the measure of the CIB.

Correlation coefficients show that the correlation is good for both colors (see Table 1). The CIB is obtained by removing the faint star contribution to the intercept value.

4.2. *Zodiacal Contamination*

Since the main error is suspected to come from the zodiacal subtraction in the DIRBE maps, a representation of the CIB versus the ecliptic latitude β is useful. For each pixel, we estimate the intercept of the DIRBE/2MASS linear correlation in a 5° radius area, and we remove the faint-star model from the DIRBE data. After this operation, we select regions with the best DIRBE/2MASS correlation, as

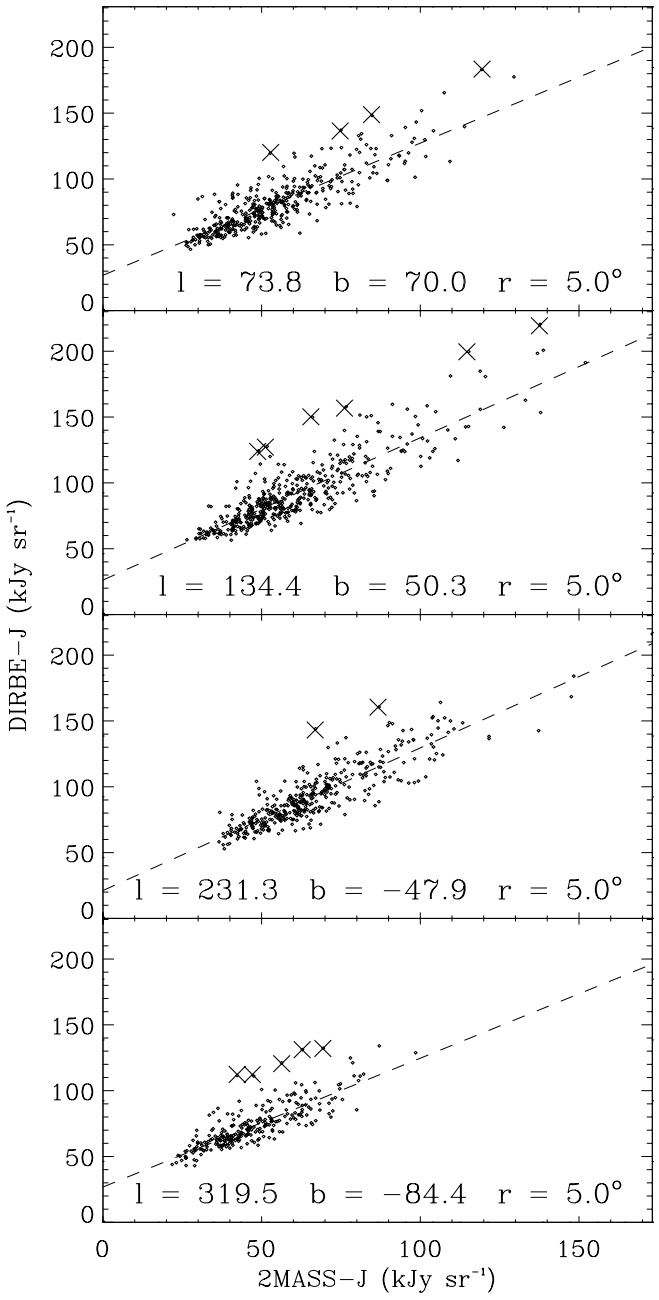

FIG. 4*a*

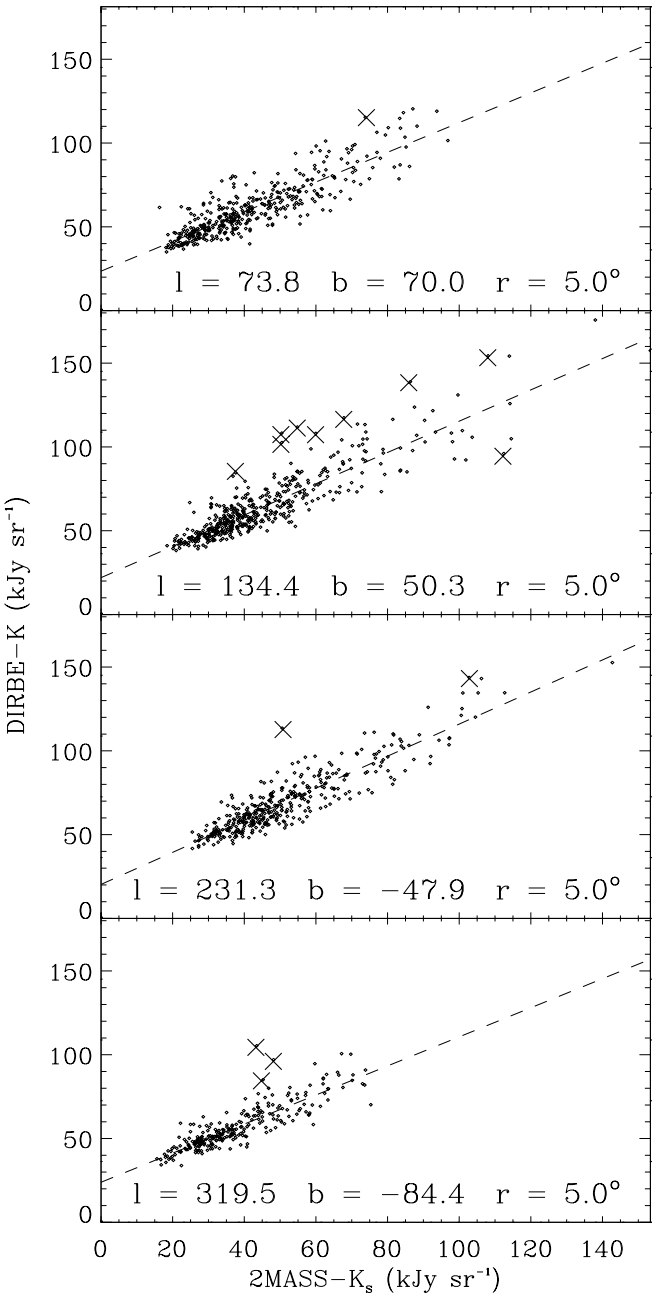

FIG. 4*b*

FIG. 4.—DIRBE vs. 2MASS for four regions of 5° radius. Pixels contaminated by bright stars have been removed. Crosses correspond to pixels rejected by the 3 σ robust fitting. See Table 1 for main characteristics.

TABLE 1

DIRBE/2MASS Correlations for the Four Areas

Band	b (deg)	l (deg)	Number of Pixels	Slope	Intercept (kJy sr^{-1})	Correlation Coefficient	Faint Stars[a] (kJy sr^{-1})	CIB (kJy sr^{-1})
J	70.02	73.84	407	1.00 ± 0.03	26.9 ± 1.6	0.87	1.44	25.5
K			409	0.89 ± 0.02	23.6 ± 1.1	0.87	1.84	22.0
J	50.30	134.42	462	1.08 ± 0.03	26.2 ± 1.7	0.88	1.68	24.4
K			472	0.93 ± 0.02	22.0 ± 1.0	0.89	2.34	19.8
J	−47.86	231.32	386	1.08 ± 0.03	21.2 ± 1.9	0.88	1.81	19.2
K			389	0.96 ± 0.02	20.3 ± 1.2	0.91	2.54	17.9
J	−84.42	319.54	263	0.98 ± 0.04	26.8 ± 1.8	0.82	1.64	25.2
K			260	0.87 ± 0.03	23.9 ± 1.1	0.86	2.05	22.1

[a] Faint star ($J > 15.8$, $K_s > 14.3$) contribution from the Jarrett model.

defined in Table 2. These values were obtained by examination of the histogram of each quantity and correspond to the peak value divided by 4. This selection leads to ~ 550 deg^2 of reliable regions in the sky.

Figure 5 shows the resulting CIB versus ecliptic latitude for both colors with an additional plot of the DIRBE 25 μm zodiacal subtracted surface brightness. For this figure, we include both low and ecliptic latitude points. The 25 μm band is the most sensitive to the zodiacal light and contains subtraction residuals from the interplanetary dust model. Comparison of the 25 μm plot with the CIB plots confirms that the scatter at low ecliptic latitude comes mainly from residual zodiacal effects.

Systematic uncertainties associated with the zero points of the interplanetary dust models are difficult to estimate. Kelsall et al. (1998) estimate them by choosing the *largest* among three models at high ecliptic latitude. Accordingly, conservative estimates of the systematic uncertainties in J and K are 6.25 kJy sr^{-1} and 4.4 kJy sr^{-1}, respectively. If the three models used to derive these numbers were equally distributed in the space of possible models, the given uncertainties would correspond to 1.6 σ. Unfortunately, the models are probably not equally probable, and it is hard to interpret these numbers in terms of a confidence level. To be conservative, we assume that they correspond to 1 σ. Theoretical uncertainties in the zodiacal light model are further discussed by Dwek et al. (1998).

Statistical uncertainties that come from the DIRBE/2MASS correlation and from the zodiacal light can be estimated directly from Figure 5 by measuring the rms deviation of the distribution. The resulting uncertainties are 2.7 kJy sr^{-1} for J and 2.1 kJy sr^{-1} for K. A summary of the different uncertainty contributions is presented in Table 3. The presence of fluctuations in the residual sky brightness, especially in J, suggests a small contribution to the sky brightness by starlight scattered off of interstellar dust grains.

TABLE 2

Selection of the Best DIRBE/2MASS Correlation Areas

Quantity	J	K
Number of pixels	≥ 80	≥ 80
Correlation coefficient.....	≥ 0.72	≥ 0.82
Mean square deviation.....	≤ 200	≤ 80
Intercept σ.....	≤ 2.8	≤ 1.6
Slope σ.....	≤ 0.05	≤ 0.035
Slope	$\in$ [0.97, 1.125]	$\in$ [0.85, 0.965]

4.3. *Local Interstellar Medium Contamination*

Interstellar dust passing through the solar system will scatter and reemit absorbed sunlight. The volume within which sunlight is significant (compared to the interstellar radiation field [ISRF]) is smaller than the size of the solar system itself: at visible wavelengths, sunlight exceeds the ISRF out to the Oort cloud ($\sim 10^4$ AU), while at far-ultraviolet wavelengths, sunlight exceeds the ISRF only out to 800 AU (at 0.2 μm) or less. The amount of interstellar dust close to the Sun was recently measured by the *Ulysses* and *Galileo* space probes (Grün et al. 1994); the volumetric cross section is $n_d \sigma_d \simeq 2.9 \times 10^{-23}$ cm^2 cm^{-3}. It was found that the size distribution is deficient in small particles relative to the interstellar size distribution, such that the surface area is dominated by particles with a size of $\simeq 0.4$ μm.

To estimate the brightness of sunlight scattered by local interstellar dust, we assume that the particles detected by *Ulysses* are spread uniformly throughout the solar system. The emission from dust in the inner solar system will have a detectable dependence on solar elongation angle and would have been included in the DIRBE zodiacal emission model (Kelsall et al. 1998). Therefore, in calculating the brightness of sunlight scattered by local interstellar dust that potentially contributes to an isotropic background, we integrate from 3 AU outward. The brightness is

$$I_{\rm LISM} = \int_3^\infty \omega n_d \sigma_d I_\odot \Phi dL ,$$

where ω is the albedo, $I_\odot$ is the solar intensity, and Φ is the scattering phase function. Using the properties of a mixture of astronomical silicates and graphite (Draine & Lee 1984), the albedo in the J and K bands is 0.42 and 0.21, respectively. For the phase function, we used a Henyey-Greenstein function with the asymmetry factor appropriate for the same mixture of astronomical silicates and graphite ($g_J = 0.15$, $g_K = 0.02$). The resulting brightness is $I_{\rm LISM} = 0.8$ and 0.3 kJy sr^{-1} in the J and K bands, respectively.

Uncertainty in the estimate of the brightness of the local interstellar dust is due to three sources. First, our lack of accurate knowledge of the interstellar grain composition leads to a factor of approximately 2 uncertainty in its albedo; this is based on the difference between the albedos of silicate and graphite grains (Draine & Lee 1984). Second, the lack of precise distinction between the emission that would be effectively isotropic and that which would be incorporated into the zodiacal light model leads to a $\sim 20\%$ uncertainty; this is based on changing the minimum integration distance from 3 to 2.5 AU. Third, smaller particles

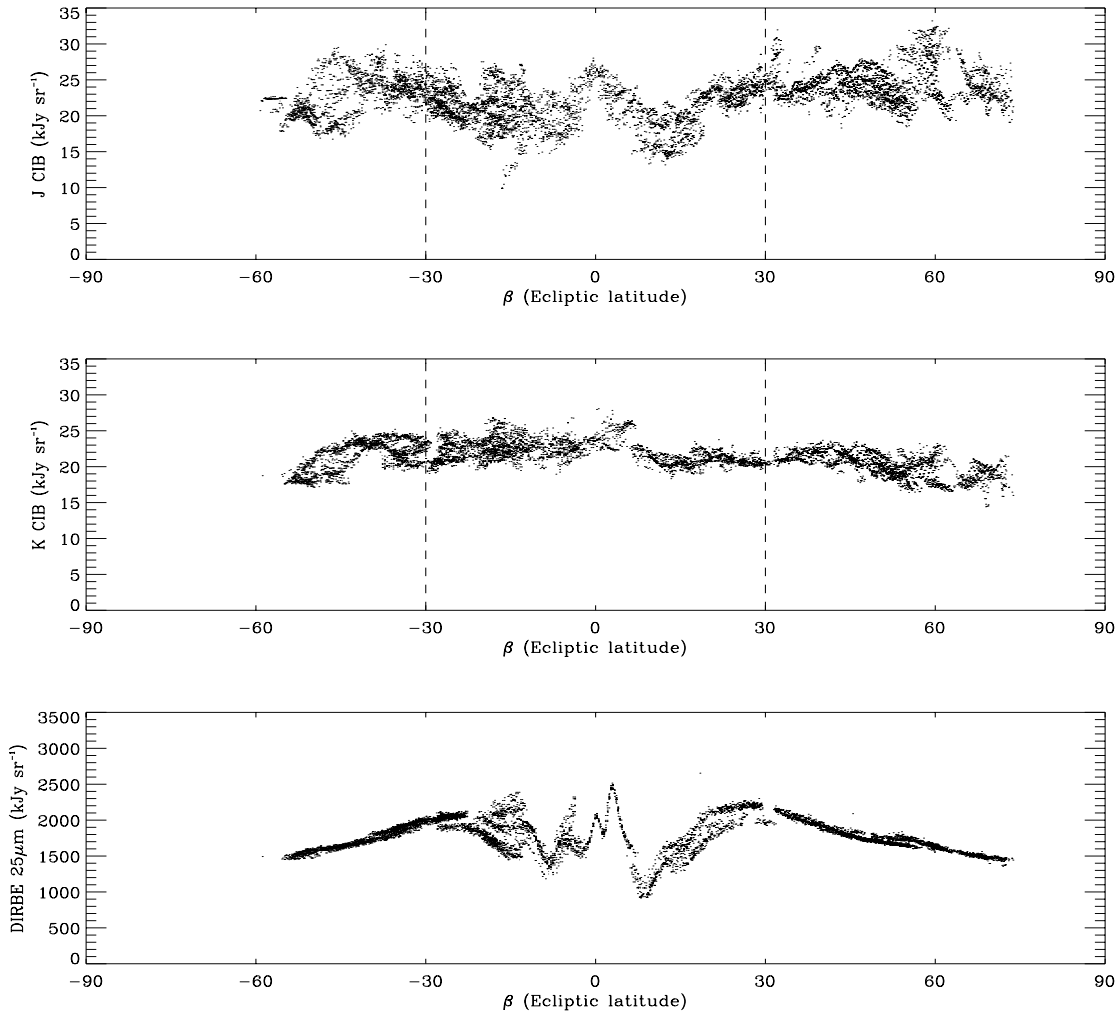

FIG. 5.—CIB vs. ecliptic latitude for J (*top*) and K (*middle*). Only pixels with Galactic $|b| > 40°$, good DIRBE/2MASS correlation, and low DIRBE 240 μm are plotted. *Bottom*: Total DIRBE flux at 25 μm vs. ecliptic latitude for comparison. The same zodiacal light subtraction features appear in the three maps. The main uncertainty comes therefore from the zodiacal light; resulting CIB values are 22.9 ± 7.0 kJy sr^{-1} (54.0 ± 16.8 nW m^{-2} sr^{-1}) and 20.4 ± 4.9 kJy sr^{-1} (27.8 ± 6.7 nW m^{-2} sr^{-1}) for J and K, respectively.

that are not detected by *Ulysses* may be present at larger distances from the Sun; these particles are likely to produce an insignificant scattering because of the weakness of sunlight at large distances from the Sun. To summarize, we estimate the CIB as follows: CIB(J) = 22.9 ± 7.0 kJy sr^{-1} (54.0 ± 16.8 nW m^{-2} sr^{-1}) and CIB(K) = 20.4 ± 4.9 kJy sr^{-1} (27.8 ± 6.7 nW m^{-2} sr^{-1}).

5. DISCUSSION

5.1. *Comparison with Previous Studies*

Previous estimations of the CIB in K are 16.4 ± 4.4 kJy sr^{-1} and 14.8 ± 4.1 kJy sr^{-1}, by Gorjian et al. (2000) and Wright (2001), respectively. The difference between these values and the estimation given in this paper

TABLE 3

UNCERTAINTIES: VALUES FOR 1 σ

Quantity	J	K
Bright stars (≤ 5 mag)	Removed	Removed
2MASS flux per DIRBE pixel ($5 < J \leq 15.8$, $5 < K_s \leq 14.3$; kJy sr^{-1})	4.2×10^{-5}	4.5×10^{-5}
Faint stars model ($J > 15.8$, $K_s > 14.3$; kJy sr^{-1})	<2	<2
DIRBE flux (kJy sr^{-1})	2.2	2.1
DIRBE/2MASS slope (%)	<10, no consequence	<10, no consequence
$K \neq K_s$	...	2.5×10^{-5}
CIB scatter (statistical uncertainty; kJy sr^{-1})	2.7	2.1
Zodiacal light model (systematic uncertainty; kJy sr^{-1})	6.25	4.4
Local interstellar medium (kJy sr^{-1})	1.6	0.6
Total CIB uncertainty (kJy sr^{-1})	7.0	4.9

is within the measurement uncertainties (1 σ) and thus is in good agreement. Most of the difference can be attributed to the zodiacal light subtraction because we used the Kelsall et al. (1998) model and they used the Wright (1998) model.

The estimation of the CIB in J can be compared to the weak limit of 12.0 ± 6.3 kJy sr^{-1} proposed by Wright (2001). The discrepancy with our value (22.9 ± 7.0 kJy sr^{-1}) can be explained by the zodiacal light subtraction, since Wright would find 25.8 kJy sr^{-1} with the Kelsall et al. (1998) interplanetary dust model.

Kashlinsky & Odenwald (2000) have investigated the CIB fluctuations in the DIRBE maps from 1.25 μm to 4.9 μm. Fluctuations on the DIRBE beam scale are expected to be 10%–20% of the total CIB flux (A. Kashlinsky 2000, private communication). Their values of $6.5^{+1.5}_{-2.9}$ and $4.3^{+1.2}_{-2.7}$ kJy sr^{-1} (92% confidence level) for J and K, respectively, are therefore in agreement with our results in both bands.

5.2. *Galaxy Counts*

Galaxy counts and the CIB are closely related: at least part of the CIB is due to the integrated surface brightness of galaxies for all redshifts. In the past decade, many efforts have been made to obtain galaxy counts in a wide range of magnitudes. T. H. Jarrett et al. (2001, in preparation) performed large-scale studies with 2MASS (2350 deg^2), which provide galaxy counts for $8 \leq J \leq 15$ and $8 \leq K_s \leq 14$. Bershady, Lowenthal, & Koo (1998) obtained ground-based observations up to 24 mag in J and K with the Keck 10 m telescope. Saracco et al. (1999) used the ESO New Technology Telescope (NTT) and obtained galaxy counts for $17 \leq J \leq 24$ and $16 \leq K \leq 22$. Deeper observations are possible with the Hubble Deep Field of the *Hubble Space Telescope* (*HST*), and Thompson et al. (1999) reached 29 and 28 mag in the *HST* filters F110W and F160W, which correspond roughly to $I + J$ and H, respectively.

Figure 6 shows the cumulative brightness of galaxies up to $J = 29$ and $K = 28$ mag. For the faintest J and K region (24–30 mag), we used the *HST* measurements, assuming $m_{\rm F110W} - m_J = 0$ and $m_{\rm F160W} - m_K = 0$. The resulting error can be neglected since the contribution of these very faint galaxies to the total brightness is small (9% of the total energy in J, only 3% in K). But note that 90% of the energy is in the ranges $12 \leq J \leq 24$ and $14 \leq K \leq 22$.

Uncertainties on galaxy counts come from the Poisson statistics ($\sigma = \sqrt{N}$) and from completeness limitations and corrections. By comparing galaxy counts in the literature, we find that the number of galaxies by range of magnitude N is consistent to within a factor of 1.75, which we adopt as a conservative value for the uncertainty. We find a J-band total brightness of 3.6 ± 0.8 kJy sr^{-1} for galaxies and a K-band total brightness of 5.3 ± 1.2 kJy sr^{-1}, which is in good agreement with Pozzetti et al. (1998), who obtained 5.8 kJy sr^{-1} in the K band.

The integrated galaxy counts are smaller than our DIRBE/2MASS CIB estimations, even compared with the 95% confidence level. We can address the possibility of large diffuse galaxy halos that would not be included in the galaxy luminosities (because of their faintness), and we find that, to reduce the discrepancy between galaxy surface brightness and our CIB value to less than 1 σ, an increase of each galaxy luminosity by a factor 3.6 and 2.4 is required in J and K, respectively. If we assume that galaxy photometries are correct, a significant part of the energy in the CIB is not detected in sources. The slope of the galaxy luminosity function is observed to flatten for $K > 17$ (Saracco et al. 1997), and the resulting slope for the cumulative brightness is almost 0 for $K > 25$ mag. For J, the slope change in the luminosity function is not as pronounced as for K, but the slope of the cumulative brightness is also close to 0 for $J > 25$. Consequently, the slope of the galaxy luminosity function must increase for fainter magnitudes or other contributions to the near-infrared background must be invoked. To summarize, the brightness of the cosmic background found in this paper (§ 4) is greater than the integrated brightness of galaxy counts by 19.3 ± 7.8 kJy sr^{-1} (46.3 ± 18.7 nW m^{-2} sr^{-1}) at J and 15.1 ± 6.1 kJy sr^{-1} (20.6 ± 8.3 nW m^{-2} sr^{-1}) at K.

5.3. *Other Possible Contributions to the CIB*

Although galaxies appear to be unable to explain the brightness of the cosmic background, there are other pos-

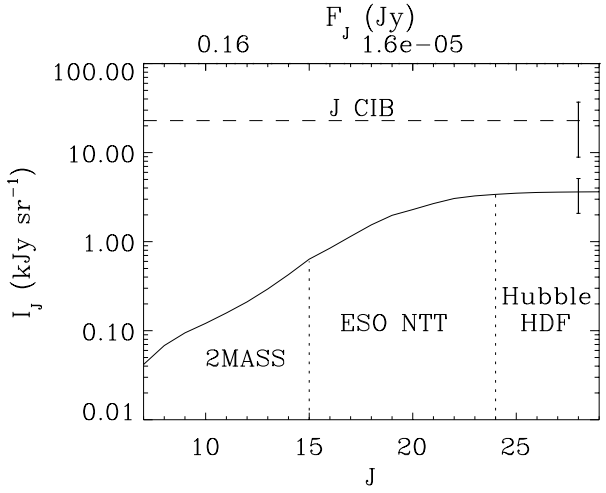

FIG. 6*a*

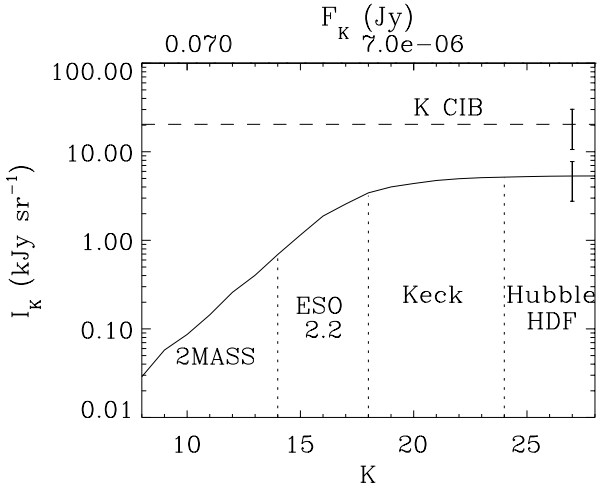

FIG. 6*b*

FIG. 6.—Comparison of the CIB with the cumulative brightness derived from galaxy counts. Data are from 2MASS (Jarrett et al. 2001, in preparation), ESO/NTT (Saracco et al. 1999), ESO 2.2 m (Saracco et al. 1997), Keck (Bershady et al. 1998), and *HST* (Thompson et al. 1999). Error bars correspond to a 95% (2 σ) confidence level. A significant part of the energy is still not detected in sources for both colors.

sible sources of energy production that could lead to an isotropic cosmic background in the near-infrared. An early burst of star formation inside or outside of galaxies (i.e., either in primeval galaxies or in Population III stars) would result in a nearly uniform and isotropic background (Bond, Carr, & Hogan 1986). The photospheric emission from these stars would be redshifted into the infrared. For $z_* \sim 10$, the background due to high-mass stars will peak at wavelengths of 1 μm, and the background due to intermediate-mass stars will be in the range 0.5–2 μm; for $z_* \sim 100$, the background due to high-mass stars will peak at wavelengths of 10 μm, and the background due to intermediate-mass stars will be in the range 0.5–6 μm. The gap between our background estimation and galaxy count contributions could be due to Population III stars. The present abundance of heavy elements limits the amount of early star formation such that Population III stars are not likely to give a very significant mass contribution to the universe as a whole (Bond et al. 1986), but the amount of star formation required to explain the near-infrared cosmic background does not violate metallicity constraints. The implications of such early star formation, for the small-scale density fluctuations of primordial matter and for the nature of the intergalactic medium, would be significant.

Depending on the power spectrum of small-scale density fluctuations, a population of black holes could form before the formation of galaxies. The accretion of surrounding material by these holes would generate energy that would make an isotropic background today. The temperature of the accretion disk would be $\sim 10^5$ K, and the accretion luminosity would be redshifted into the near-infrared if the accretion is active at $z_{bh} \sim 30$–50 (Carr 1994). Our observed J-band background brightness, after subtracting the integrated light from galaxies, could be explained by the accretion luminosity of a population of black holes. Such black holes would not comprise enough dark matter to close the universe, and their total mass would not violate constraints on the total baryon density inferred from models of primordial nucleosynthesis, but such a large population of objects (comparable to the total mass of galaxies) would contribute significantly to the total inventory of baryons.

Massive particles that survive until redshift z_ν then subsequently decay into photons will produce a background of decay photons that is subsequently redshifted (Bond et al. 1986). For example, part of the J- and K-band background could be produced by the decay of relic 100 eV neutrinos at redshift $z_\nu \sim 300$. The number of plausible models is very large, and we can only speculate whether the background is due to such decaying particles.

6. CONCLUSION

The integration of the 2MASS catalog over 550 deg^2 (i.e., $\sim$5500 DIRBE pixels) leads to an estimate of the CIB for J and K of 22.9 ± 7.0 kJy sr^{-1} (54.0 ± 16.8 nW m^{-2} sr^{-1}) and 20.4 ± 4.9 kJy sr^{-1} (27.8 ± 6.7 nW m^{-2} sr^{-1}), respectively.

We have selected the most reliable areas of the sky by eliminating pixels contaminated by bright stars, low Galactic latitude regions, low ecliptic latitude regions, and possible cirrus cloud contribution. A study of DIRBE$-$2MASS versus ecliptic latitude clearly shows that the zodiacal light is responsible for most of the statistical uncertainty ($\sim$2 kJy sr^{-1}). The interplanetary dust model contains a systematic error, which is actually the dominant uncertainty in our results ($\sim$5 kJy sr^{-1}).

The integrated brightness of known galaxies (down to $\sim$29 mag) represents only a fraction of the CIB. Although the uncertainties due to residual contribution of the zodiacal light are significant, the discrepancy between DIRBE$-$2MASS and galaxy counts would suggest that a significant part of the energy is still not observed in discrete sources. The slope of the galaxy luminosity functions may increase for galaxies fainter than 30 mag, in which case the counts would agree with the CIB values. However, models predict other possible contributions to the background at these wavelengths (Bond et al. 1986) such as a burst of star formation in primeval galaxies or in Population III stars ($z \approx 10$), very massive black holes (accreting from an uniform pregalactic medium at $z \approx 40$), or massive decaying big bang relic particles ($z \approx 300$). We have put new constraints on the near-infrared that encourage revisiting the importance of those contributions to the CIB in cosmological models.

The Space Infrared Telescope Facility may extend this result for the L band at 3.5 μm and might be able to constrain the contributions of the different components to the background.

The final 2MASS catalogs will permit a more accurate study of the near-infrared excess: 100% of the sky will still be available after integration on the DIRBE beam, $\sim$75% after bright star removal (only 18% for the 2MASS Second Release presently used), and about 5000 deg^2 at high Galactic and ecliptic latitudes. This coverage should allow us to investigate structures in the zodiacal light and may help to improve interplanetary dust models.

We are grateful to Roc Cutri for his help in accessing the 2MASS data and for his critical reading of this paper and to George Helou for helpful discussions. This publication makes use of data products from 2MASS, which is a joint project of the University of Massachusetts and the Infrared Processing and Analysis Center/California Institute of Technology, funded by NASA and NSF. The *COBE* data sets were developed by the NASA Goddard Space Flight Center under the guidance of the *COBE* Science Working Group and were provided by the NSSDC. L. Cambrésy acknowledges partial support from the Lavoisier grant of the French Ministry of Foreign Affairs.

REFERENCES

Arendt, R. G., et al. 1998, ApJ, 508, 74
Bahcall, J. N., & Soneira, R. M. 1980, ApJS, 44, 73
Bershady, M. A., Lowenthal, J. D., & Koo, D. C. 1998, ApJ, 505, 50
Bond, J. R., Carr, B. J., & Hogan, C. J. 1986, ApJ, 306, 428
Campins, H., Rieke, G. H., & Lebofsky, M. J. 1985, AJ, 90, 896
Carr, B. 1994, ARA&A, 32, 531
Cutri, R. M., et al. 2000, Explanatory Supplement to the 2MASS Second Incremental Data Release
Draine, B. T., & Lee, H. M. 1984, ApJ, 285, 89
Dwek, E., & Arendt, R. G. 1998, ApJ, 508, L9
Dwek, E., et al. 1998, ApJ, 508, 106
Elias, J. H. 1978, ApJ, 223, 859
Gardner, J. P., Sharples, R. M., Frenk, C., & Carrasco, B. 1997, ApJ, 480, L99
Garwood, R., & Jones, T. 1987, PASP, 99, 453
Gispert, R., Lagache, G., & Puget, J.-L. 2000, A&A, 360, 1
Gorjian, V., Wright, E. L., & Chary, R. R. 2000, ApJ, 536, 550
Grün, E., Gustafson, B., Mann, I., Baguhl, M., Morfill, G. E., Staubach, P., Taylor, A., & Zook, H. A. 1994, A&A, 286, 915
Hauser, M. G., et al. 1998a, ApJ, 508, 25

Hauser, M. G., Kelsall, T., & Weiland, J. 1998b, *COBE* Diffuse Infrared Background Experiment Explanatory Supplement (*COBE* Ref. 98-A; Greenbelt: NASA/GSFC)
Jarrett, T. H. 1992, Ph.D. thesis, Univ. Massachusetts, Amherst
Jones, T. J., Ashley, M., Hyland, A. R., & Ruelas-Mayorga, A. 1981, MNRAS, 197, 413
Kashlinsky, A., & Odenwald, S. 2000, ApJ, 528, 74
Kelsall, T., et al. 1998, ApJ, 508, 44
Lagache, G., Haffner, L. M., Reynolds, R. J., & Tufte, S. L. 2000, A&A, 354, 247
Matsumoto, T., et al. 2000, Proc. of *ISO* Surveys of a Dusty Universe (Ringberg Castle: ISO)
Pahre, M. A., & Mould, J. R. 1994, ApJ, 433, 567
Persson, S. E., Murphy, D. C., Krzeminski, W., Roth, M., & Rieke, M. J. 1998, AJ, 116, 2475
Pozzetti, L., Madau, P., Zamorani, G., Ferguson, H. C., & Bruzual, A. G. 1998, MNRAS, 298, 1133
Puget, J.-L., Abergel, A., Bernard, J.-P., Boulanger, F., Burton, W., Desert, F.-X., & Hartmann, D. 1996, A&A, 308, L5
Saracco, P., D'Odorico, S., Moorwood, A., Buzzoni, A., Cuby, J.-G., & Lidman, C. 1999, A&A, 349, 751
Saracco, P., Iovino, A., Garilli, B., Maccagni, D., & Chincarini, G. 1997, AJ, 114, 887
Thompson, R. I., Storrie-Lombardi, L. J., Weymann, R. J., Rieke, M. J., Schneider, G., Stobie, E., & Lytle, D. 1999, AJ, 117, 17
Wainscoat, R. J., & Cowie, L. L. 1992, AJ, 103, 332
Wright, E. L. 1998, ApJ, 496, 1
———. 2001, ApJ, 553, 538